Earth ArXiv

Peer review status:

This is a non-peer-reviewed preprint submitted to EarthArXiv.

# Mapping Rock Density in Ireland via Image-Based Geological Classification and Geodetic Modeling

Marco Gameiro

Polytechnic of Leiria
June 2025

**Abstract**

This study presents a comprehensive geospatial and geophysical workflow designed to develop a detailed rock density model for Ireland. The methodology integrates image-based classification of geological maps, specifically from the Geological Survey of Ireland (GSI), with precise geodetic computations. We detail the procedures for classifying rock types based on RGB values, assigning accurate geographic coordinates (WGS84 and Irish Transverse Mercator - ITM), and computing crucial elevation data including ellipsoidal, geoid, and orthometric heights. A Digital Elevation Model (DEM) is then generated through interpolation using the derived height information. The resultant multi-dimensional dataset provides spatial, geological, and comprehensive elevation attributes for each processed pixel across the entire Irish landmass. This innovative approach offers a data-driven solution for large-scale geological characterization, which is fundamental for diverse Earth science applications, including accurate geoid modeling, gravimetric data interpretation, resource management, geotechnical assessments, and environmental planning. The paper elucidates the methodologies, presents the initial results, and discusses current implementation considerations and future directions for enhancing model precision.

## 1 Introduction

Understanding the Earth's crustal structure and its physical properties, particularly rock density and geological distribution, is of paramount importance for a vast array of scientific and engineering applications. These range from accurate geoid modeling and gravimetric data interpretation to vital considerations in environmental planning, resource management, and seismic risk modeling [1, 9]. The precise determination of orthometric heights and the modeling of the geoid from gravimetric data critically rely on detailed digital terrain models (DTMs) and, crucially, accurate subsurface rock density models (DDMs) to correctly compute topographical effects [11, 10, 9].

Historically, a constant topographic density value, as first proposed by Hayford [3], has been widely adopted in geodetic computations. However, recent research has consistently demonstrated that this assumption can lead to significant inaccuracies, particularly in mountainous regions. Studies have reported that such a constant value may be overestimated, with average continental crust densities found to be around 2440 $kg \cdot m^{-3}$ for New Zealand [9] and 2459 $kg \cdot m^{-3}$ for Brazil [2]. The continued reliance on a generalized, often rough, estimation of constant topographic density can introduce errors at the decimeter level in orthometric height determination and geoid modeling [4, 5, 6, 7, 8]. To address these challenges and support the ongoing modernization of height systems, the development of detailed DDMs has become an imperative [11, 10].

This study aims to contribute to this critical need by providing a detailed rock density model for Ireland. We present a novel, data-driven geospatial workflow that seamlessly integrates image-based geological classification with advanced geodetic height modeling. Unlike conventional approaches that often focus on singular geophysical parameters, our research distinguishes itself by concurrently modeling a comprehensive suite of attributes for each processed pixel across the entire Irish landmass. This includes not only detailed geological classification and estimated rock density but also precise WGS84 and Irish Transverse Mercator (ITM) coordinates, along with a full spectrum of elevation data comprising ellipsoidal, geoid, and orthometric heights, and pixel coverage. This holistic, multi-dimensional dataset offers a significantly richer characterization of the subsurface, which is paramount for enhancing the accuracy of various downstream applications, such as more reliable seismic risk modeling, improved understanding of potential ground motion for infrastructure planning, and robust hydrological modeling for effective flood risk assessment and urban development.

This project originated as part of a Short Advanced Program (SAP) in Limerick, Ireland, and was subsequently continued independently for a period of 10 months. Our methodology leverages readily available open data, specifically a digital geological map provided by the Geological Survey of Ireland (GSI), combined with powerful open-source geoprocessing techniques implemented in Python. The subsequent sections of this paper will systematically detail the data and materials utilized, comprehensively outline the image classification, coordinate assignment, and height modeling methodologies, present the initial results obtained, and conclude with a discussion of the implications, current implementation considerations, and avenues for future research.

# 2 Data and Materials

The primary input for this study was a digital geological map obtained from the Geological Survey of Ireland (GSI), specifically the 'Bedrock' section of their publicly available maps. This map served as the foundational dataset for the image-based geological classification and subsequent spatial analysis. Additional input included a CSV file detailing the location and count of grid line pixels to be excluded from analysis.

The computational workflow was developed using Python, leveraging several key libraries. **OpenCV (Open Source Computer Vision Library)** was utilized for its robust image processing capabilities. **PyProj** was essential for geodetic computations, facilitating comprehensive coordinate transformations between different reference systems and allowing for the accurate querying of geoid models. **NumPy** was used for efficient numerical operations and array manipulation. Additionally, **Pandas** was employed for data manipulation and analysis. **Pillow (PIL)** was used for image resizing and basic image operations. **Rasterio** and **SciPy** were used for generating and saving the Digital Elevation Model (DEM) through interpolation. All processed information, including geological and geodetic attributes for each pixel, was systematically saved in a `.db` (database) file, employing a chunk-based approach to efficiently manage and store the large volume of generated data.

# 3 Methodology

The overall methodology was implemented through a series of Python scripts, orchestrating specialized modules for image processing, coordinate transformations, geoid and ellipsoidal height computations, DEM generation, database management, and coverage calculations.

## 3.1 Data Pre-processing and Image Classification

The initial step involved preparing the input geological map image for analysis. The image was first resized to a target pixel count while maintaining its aspect ratio. This scaling factor, $s$, was calculated based on the target number of pixels ($P_{target}$) and the original image dimensions ($W_{orig}$, $H_{orig}$):

$$s = \sqrt{\frac{P_{target}}{W_{orig} \times H_{orig}}} \tag{1}$$

The new dimensions ($W_{new}$, $H_{new}$) were then determined by applying this scaling factor:

$$W_{new} = W_{orig} \times s, \quad H_{new} = H_{orig} \times s \tag{2}$$

Subsequently, an analysis of grid line pixels, which were identified from a CSV file, was performed. These pixels, accounting for approximately 0.163% of the total image area, were carefully excluded from the analysis to prevent distortion in geological interpretations and coverage calculations. These ignored pixel coordinates were loaded from the CSV, and then marked as transparent within the image, ensuring they were not included in subsequent geological classification.

For each remaining pixel, its RGB values ($R_p, G_p, B_p$) were extracted and compared with a set of predefined RGB values ($R_l, G_l, B_l$) from the map's legend, representing various rock types. These reference RGB values were obtained through an automated process utilizing an external large language model to identify specific color codes, which were subsequently saved in a dictionary data structure. The classification was performed by calculating the Euclidean distance ($d$) between a pixel's RGB triplet and each legend entry's RGB triplet:

$$d = \sqrt{(R_p - R_l)^2 + (G_p - G_l)^2 + (B_p - B_l)^2} \tag{3}$$

The rock type corresponding to the minimum Euclidean distance was assigned to the pixel. No explicit cutoffs for Euclidean distance were applied, meaning every pixel was assigned the closest rock type based on color similarity. While geological maps may contain non-geological features such as roads or water bodies, these were considered to represent a minor portion of the overall territory, and thus no specific masking was applied for these elements during the RGB classification.

## 3.2 Coordinate Assignment

For each classified pixel, its spatial location was determined. Latitude and longitude matrices were generated based on the image dimensions and known geographic extent. This geographic extent (minimum and maximum WGS84 longitude and latitude) was determined by observational geo-referencing within QGIS software. WGS84 geographic coordinates (latitude and longitude) were assigned to the center of each pixel by linearly distributing the minimum to maximum latitude and longitude values across the image dimensions. These WGS84 coordinates (EPSG:4326) were then transformed into the Irish Transverse Mercator (ITM) projection (EPSG:2157) using the `pyproj` library. ITM was specifically chosen because it is the designated national coordinate system for Ireland, optimized to provide the highest accuracy for planar distance and area calculations across the country.

## 3.3 Height Modeling and DEM Generation

Height modeling involved computing ellipsoidal and geoid heights for each pixel, which were then used to derive orthometric heights.

Ellipsoidal heights ($h$) were computed by transforming the Earth-Centered, Earth-Fixed (X, Y, Z) coordinates to a 3D geographic coordinate system that inherently includes ellipsoidal height. The (X, Y, Z) coordinates are derived from WGS84 geographic coordinates using a 'pyproj' transformer from 'EPSG:4326' to 'EPSG:4979'. Subsequently, 'pyproj.Transformer' is used to convert from 'EPSG:4979' (WGS84 Geocentric CRS) to 'EPSG:4978' (WGS84 Geographic 3D CRS), which provides the ellipsoidal height as part of its output. This approach ensures a precise determination of height above the WGS84 ellipsoid surface. The implementation of this calculation was performed in Python using the `pyproj` library.

Geoid heights ($N_g$) were computed using a spherical harmonic expansion method based on a global geopotential model. The general formula for the geoid undulation is given by:

$$N_g = \frac{GM}{\gamma_0 r} \sum_{n=2}^{N_{max}} \left(\frac{a}{r}\right)^n \sum_{m=0}^{n} (\bar{C}_{nm} \cos(m\lambda) + \bar{S}_{nm} \sin(m\lambda)) \bar{P}_{nm}(\sin \bar{\phi}) \tag{4}$$

where $GM$ is the geocentric gravitational constant, $\gamma_0$ is the normal gravity, $a$ is the semi-major axis, $r$ is the local ellipsoidal radius, $\lambda$ is the longitude, $\bar{C}_{nm}$ and $\bar{S}_{nm}$ are the fully normalized spherical harmonic coefficients, and $\bar{P}_{nm}(\sin \bar{\phi})$ are the fully normalized associated Legendre functions evaluated at the sine of the geocentric latitude $\bar{\phi}$. This computation was implemented in Python.

The orthometric height H was then calculated as the difference between the ellipsoidal height and the geoid height:

$$H = h - N_g \tag{5}$$

This calculation correctly combines the precisely determined ellipsoidal heights and the computed geoid heights to derive orthometric heights relative to the geoid.

A Digital Elevation Model (DEM) was generated from the computed orthometric heights. This involved interpolating the scattered latitude, longitude, and height data onto a regular grid using cubic interpolation (from `scipy.interpolate.griddata`). The generated DEM was then saved to a GeoTIFF file.

### 3.4 Rock Density Assignment and Coverage Calculation

For each identified rock type, an average rock density value was assigned. This process involved associating the classified geological unit with pre-determined average densities, which are crucial for interpreting the geomechanical properties of the rock formations and are detailed in the Results section (Table 1).

Rock type coverage was computed by counting the pixels classified as each rock type and expressing this count as a percentage of the total non-ignored pixels:

$$\text{Coverage}(\%) = \left( \frac{\text{Number of pixels for rock type}}{\text{Total number of analyzed pixels}} \right) \times 100 \tag{6}$$

The computed coverage results were then saved to an Excel file.

### 3.5 Data Management

All processed geospatial data, including latitudes, longitudes, easting, northing, geoid heights, and ellipsoidal heights, were systematically saved to an SQLite database (`geospatial_data.db`). The data was flattened into a tabular format before being written to the database, ensuring efficient storage and retrieval.

## 4 Results

The application of the methodology resulted in a comprehensive dataset characterizing the rock density distributions and associated geospatial attributes across Ireland. For each pixel, the dataset now contains its classified rock type, WGS84 coordinates, ITM coordinates, ellipsoidal height, geoid height, orthometric height, and assigned rock density.

Table 1 presents the average densities for the extensive list of rock types used in the analysis. These densities are crucial for interpreting the geomechanical properties of the rock formations and are fundamental for various Earth science applications.

Table 1: Average densities of rock types used in the analysis

| **Rock Type** | **Average Density (g/cm$^3$)** |
|---|---|
| Paleogene to Neogene sediments | 2.3 |
| Neogene sedimentary material | 2.4 |
| Paleocene basalt | 2.9 |
| Paleogene limestone & claystone | 2.6 |
| Upper Cretaceous limestone | 2.7 |
| Upper Jurassic mudstone & sandstone | 2.5 |
| Middle Jurassic limestone & mudstone | 2.6 |
| Lower Jurassic mudstone & limestone | 2.5 |
| Middle to Upper Triassic mudstone, sandstone, evaporite | 2.4 |
| Triassic to Cretaceous sandstone, mudstone, limestone | 2.5 |
| Mesozoic sedimentary rocks | 2.5 |
| Permian to Triassic sandstone & mudstone | 2.4 |
| Upper Paleozoic to Mesozoic sedimentary rocks | 2.5 |
| Pennsylvanian sandstone, mudstone, coal | 2.3 |
| Mississippian limestone & calcareous shale | 2.6 |
| Mississippian sandstone, mudstone, limestone | 2.5 |
| Devonian sandstone & conglomerate | 2.5 |
| Silurian sandstone & mudstone | 2.4 |
| Ordovician to Silurian sandstone & mudstone | 2.4 |
| Ordovician to Devonian granitoid & other igneous rocks | 2.7 |
| Ordovician sandstone, slate & volcanic rocks | 2.7 |
| Cambrian sandstone & quartzite | 2.65 |
| Lower Paleozoic metasedimentary rocks | 2.8 |
| Neoproterozoic schist & gneiss | 2.9 |
| Paleoproterozoic gneiss | 2.9 |
| Ordovician granitic rocks | 2.7 |
| Oligocene clay, sand & lignite | 2.2 |
| Upper Cretaceous chalk, flint, glauconitic sandstone | 2.3 |
| Tournaisian limestone | 2.6 |
| Siluro-Devonian granitic rocks & appinite | 2.7 |
| Lower to Middle Ordovician slate, sandstone, greywacke | 2.7 |
| Silurian sandstone, siltstone, conglomerate | 2.5 |
| Serpentinic & sedimentary mélange (Paleozoic) | 2.9 |
| Lower Paleozoic granitoid - dioritic rocks | 2.8 |
| Paleogene basic intrusive rocks | 2.9 |
| Paleogene rhyolite | 2.7 |
| Paleogene granitic rocks | 2.7 |
| Neoproterozoic (to Cambrian?) metasedimentary rocks | 2.8 |
| Ordovician volcanic rocks | 2.8 |
| Cambrian greywacke, slate, quartzite | 2.7 |
| Mesoproterozoic gneiss | 2.9 |
| Paleoproterozoic to Mesoproterozoic gneiss & schist | 2.9 |

Table 2 presents the RGB color codes used for classifying each rock type, directly derived from the GSI map legend. This mapping is central to the image-based classification methodology.

Table 2: RGB Color Codes for Rock Types

| **Rock Type** | **Red (R)** | **Green (G)** | **Blue (B)** |
|---|---|---|---|
| Paleogene to Neogene sediments | 255 | 218 | 185 |
| Neogene sedimentary material | 255 | 228 | 181 |
| Paleocene basalt | 255 | 99 | 71 |
| Paleogene limestone & claystone | 255 | 215 | 0 |
| Upper Cretaceous limestone | 255 | 140 | 0 |
| Upper Jurassic mudstone & sandstone | 240 | 230 | 140 |
| Middle Jurassic limestone & mudstone | 244 | 164 | 96 |
| Lower Jurassic mudstone & limestone | 188 | 143 | 143 |
| Middle to Upper Triassic mudstone, sandstone, evaporite | 184 | 134 | 11 |
| Triassic to Cretaceous sandstone, mudstone, limestone | 218 | 165 | 32 |
| Mesozoic sedimentary rocks | 210 | 105 | 30 |
| Permian to Triassic sandstone & mudstone | 222 | 184 | 135 |
| Upper Paleozoic to Mesozoic sedimentary rocks | 139 | 69 | 19 |
| Pennsylvanian sandstone, mudstone, coal | 205 | 133 | 63 |
| Mississippian limestone & calcareous shale | 210 | 180 | 140 |
| Mississippian sandstone, mudstone, limestone | 255 | 160 | 122 |
| Devonian sandstone & conglomerate | 244 | 164 | 96 |
| Silurian sandstone & mudstone | 205 | 92 | 92 |
| Ordovician to Silurian sandstone & mudstone | 255 | 69 | 0 |
| Ordovician to Devonian granitoid & other igneous rocks | 165 | 42 | 42 |
| Ordovician sandstone, slate & volcanic rocks | 128 | 0 | 0 |
| Cambrian sandstone & quartzite | 112 | 128 | 144 |
| Lower Paleozoic metasedimentary rocks | 47 | 79 | 79 |
| Neoproterozoic schist & gneiss | 95 | 158 | 160 |
| Paleoproterozoic gneiss | 0 | 206 | 209 |
| Ordovician granitic rocks | 173 | 255 | 47 |
| Oligocene clay, sand & lignite | 255 | 250 | 205 |
| Upper Cretaceous chalk, flint, glauconitic sandstone | 135 | 206 | 250 |
| Tournaisian limestone | 64 | 224 | 208 |
| Siluro-Devonian granitic rocks & appinite | 154 | 205 | 50 |
| Lower to Middle Ordovician slate, sandstone, greywacke | 255 | 192 | 203 |
| Silurian sandstone, siltstone, conglomerate | 128 | 128 | 0 |
| Serpentinic & sedimentary mélange (Paleozoic) | 218 | 112 | 214 |
| Lower Paleozoic granitoid - dioritic rocks | 255 | 127 | 80 |
| Paleogene basic intrusive rocks | 255 | 105 | 180 |
| Paleogene rhyolite | 199 | 21 | 133 |
| Paleogene granitic rocks | 255 | 99 | 71 |
| Neoproterozoic (to Cambrian?) metasedimentary rocks | 70 | 130 | 180 |
| Ordovician volcanic rocks | 147 | 112 | 219 |
| Cambrian greywacke, slate, quartzite | 240 | 128 | 128 |
| Mesoproterozoic gneiss | 0 | 255 | 255 |
| Paleoproterozoic to Mesoproterozoic gneiss & schist | 255 | 0 | 255 |

The processed output includes spatial and geological attributes for each pixel, forming a comprehensive dataset. A subset of this data, illustrating the geographic and elevation attributes, is shown in Table 3. The corresponding rock type and density properties for similar data points are presented in Table 4.

Table 3: Geographic and Elevation Data

| **Lat** | **Lon** | **Northing** | **Easting** | **GeoidHeight (m)** | **Ellip.Height(m)** | **Orth.Height(m)** |
|---|---|---|---|---|---|---|
| 51.4 | -10.4494 | 519210.2669 | 519210.2669 | -2818.2618 | -2724.2618 | 94 |
| 51.4 | -10.4488 | 519208.9869 | 429623.9351 | -2818.2618 | -2816.2618 | 2 |
| 51.4 | -10.4483 | 519207.7071 | 429662.2296 | -2818.2618 | -2816.2618 | 2 |
| 51.4 | -10.4477 | 519206.4277 | 429700.5241 | -2818.2618 | -2792.2618 | 26 |
| 51.4 | -10.4472 | 519205.1485 | 429738.8187 | -2818.2618 | -2812.2618 | 6 |
| 51.4 | -10.4466 | 519203.8696 | 429777.1132 | -2818.2618 | -2762.2618 | 56 |
| 51.4 | -10.4461 | 519202.5910 | 429815.4077 | -2818.2618 | -2778.2618 | 40 |
| 51.4 | -10.4455 | 519201.3127 | 429853.7022 | -2818.2618 | -2800.2618 | 18 |
| 51.4 | -10.4450 | 519200.0347 | 429891.9968 | -2818.2618 | -2764.2618 | 54 |
| 51.4 | -10.4444 | 519198.7569 | 429930.2913 | -2818.2618 | -2790.2618 | 28 |

Table 4: Rock Properties Data

| **Lat** | **Lon** | **Rock Type** | **RockDensity(kg/m$^3$)** | **Coverage** |
|---|---|---|---|---|
| 51.4 | -10.4494 | Lower to Middle Ordovician slate, sandstone, greyw | 2.7 | 7.3184 |
| 51.4 | -10.4488 | Lower to Middle Ordovician slate, sandstone, greyw | 2.7 | 7.3184 |
| 51.4 | -10.4483 | Lower to Middle Ordovician slate, sandstone, greyw | 2.7 | 7.3184 |
| 51.4 | -10.4477 | Lower to Middle Ordovician slate, sandstone, greyw | 2.7 | 7.3184 |
| 51.4 | -10.4472 | Lower to Middle Ordovician slate, sandstone, greyw | 2.7 | 7.3184 |
| 51.4 | -10.4466 | Lower to Middle Ordovician slate, sandstone, greyw | 2.7 | 7.3184 |
| 51.4 | -10.4461 | Lower to Middle Ordovician slate, sandstone, greyw | 2.7 | 7.3184 |
| 51.4 | -10.4455 | Lower to Middle Ordovician slate, sandstone, greyw | 2.7 | 7.3184 |
| 51.4 | -10.4450 | Lower to Middle Ordovician slate, sandstone, greyw | 2.7 | 7.3184 |
| 51.4 | -10.4444 | Lower to Middle Ordovician slate, sandstone, greyw | 2.7 | 7.3184 |

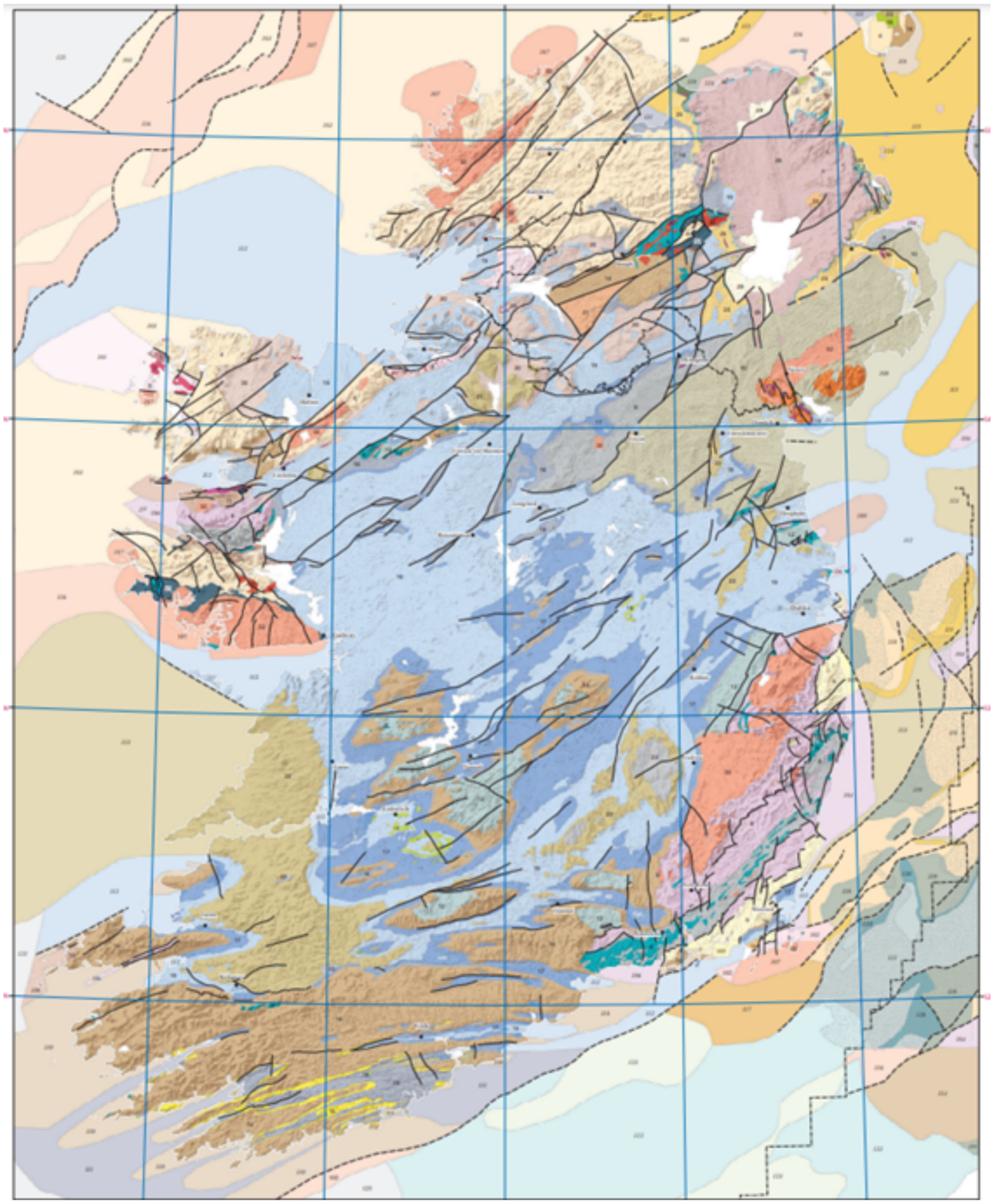

Figure 1: Classified geological map from the GSI showing various rock types across Ireland.

# 5 Discussion

The classification method offers a novel, image-based approach to geological mapping, leveraging readily available map resources. While pixel classification based on RGB values has inherent limitations, such as sensitivity to color variations in the source image or subtle differences between geological units, the integration of rigorous geodetic modeling significantly increases its utility for real-world applications by providing accurate spatial and vertical positioning. This combination of visual classification with precise geodetic computations allows for a more comprehensive understanding of the subsurface.

## 5.1 Implementation Considerations and Limitations

It is important to acknowledge certain considerations and limitations within the current implementation. Future improvements will aim to integrate a high-resolution DEM as the definitive source for orthometric heights, which can then be used to derive ellipsoidal heights given a geoid model.

The RGB-based classification method, while efficient for large-scale mapping, is sensitive to color variations inherent in the source image and subtle differences between geological units. While non-geological features like roads and water bodies were assumed to have minimal impact due to their small proportion of the landmass, precise applications might benefit from dedicated masking.

# 6 Conclusion

This project successfully developed and implemented a replicable, geospatial method for characterizing rock density distributions across Ireland. By integrating image-based geological classification with advanced geodetic modeling techniques, we have demonstrated a data-driven approach to creating detailed geological datasets. Although the formal collaboration that initiated this project concluded in March 2025, the methodology and results are made public to serve as a foundation for future research and applications in geological mapping and geophysical studies. Future work will focus on integrating external DEM data for more precise orthometric height determination.

# Acknowledgments

This work was carried out independently. I wish to express my gratitude for the initial guidance received from Professor Sajjad and for the international research opportunity provided by the Short Advanced Program (SAP) at the Technological University of the Shannon: Midlands Midwest, which laid the foundation for this project.

# References

[1] M.A. Al-Dujaili, A.S.B. Othman, A.S.O. Othman, and R.Z.A. Abed. Orthometric height using geometric-gravimetric method and gravity reduction. *Journal of Engineering Science and Technology*, 2:54–61, 2016.

[2] L.P. Fortes, E.G. Moreira, L.E.C. Paes, A.F.C.R.S. da Rocha, and J.C.F. da Silva. Gravity field modeling and density estimation using a digital terrain model and airborne gravity data for an area in the brazilian amazon. *Journal of Geodesy*, 90:137–152, 2016.

[3] John F. Hayford. *The Figure of the Earth and Isostasy from Measurements in the United States*. U.S. Coast and Geodetic Survey, 1909.

[4] M.S.E. Mohamed. A simple approach for modeling the topographic-isostatic geoid. *Journal of Geodesy*, 88:969–979, 2014.

[5] P. Novák. The effect of topographic density variations on the gravity field and its gradients. *Geodesy and Cartography*, 30:54–61, 2004.

[6] P. Novák. The effect of topographic density variations on the gravity field and its gradients. *Geodesy and Cartography*, 30:54–61, 2004.

[7] P. Novák. The effect of topographic density variations on the gravity field and its gradients. *Geodesy and Cartography*, 30:54–61, 2004.

[8] P. Novák, R. Tenzer, and L.K.M.L.K.S. Li. The effect of topographic density variations on the gravity field and its gradients. *Journal of Geodesy*, 80:249–258, 2006.

[9] Robert Tenzer, Pascal Sirguey, Mark Rattenbury, and Julia Nicolson. A digital rock density map of new zealand. *Computers & Geosciences*, 37(8):1181–1191, 2011.

[10] P. Vanicek, P. Novák, and Z. Martinec. Geoid, topography, and the bouguer anomaly. *Journal of Geodesy*, 79:129–137, 2005.

[11] Petr Vanicek and Edward J Krakiwsky. *Geodesy the concepts*. Elsevier, 2015.